nature communications

Article

https://doi.org/10.1038/s41467-025-67521-x

Feldspar reduces fault frictional healing rate under hydrothermal conditions

Received: 10 March 2025

Accepted: 1 December 2025

Published online: 23 December 2025

Check for updates

Wei Feng[1,2,5,6], Wenzhou Wang[3,6], Lu Yao[2,6] ✉, Rodrigo Gomila[1], Shengli Ma[2], Qunyang Li[3] ✉ & Giulio Di Toro[1,4] ✉

Fault restrengthening after earthquakes enables country rocks to restore elastic strain energy for subsequent seismic cycles. It originates from the contribution of several processes resulting in fault sealing and fault frictional healing, the latter arising from contact area growth and formation of new chemical bonds between grains. Laboratory studies demonstrate that fault frictional healing typically increases logarithmically with time during quasi-stationary contact (i.e., positive healing rate). Here we show that this logarithmic healing does not hold under certain (hydrothermal) conditions for feldspar, the most abundant mineral in the Earth's crust, and for common feldspar-rich rocks. The healing rate switches from positive to negative with increasing quasi-stationary contact time at temperatures ≥ 200 °C in the presence of pressurized water. This unusual healing behavior suggests that thermally-activated friction weakening processes may exist at feldspar interfaces. This hypothesis is further validated through nano-scale friction experiments by sliding single-feldspar crystals on a feldspar substrate. Given the abundance of feldspars in the Earth's crust, their peculiar healing behavior under hydrothermal conditions can lead to unexpected variations in fault strength, changing our understanding of fault mechanics and the seismic cycle, and challenging the direct extrapolation of laboratory-derived healing parameters to natural earthquake recurrence intervals.

Fault healing is a well-documented phenomenon that describes the time-dependent recovery of fault strength between earthquakes[1–6]. Fault healing is due to the contribution of several physical and chemical processes that lead to (1) fault sealing (mineral dissolution and precipitation, vein deposition, etc., and in extreme cases, fault welding by solidification of seismic friction melts)[7–10], (2) fault frictional healing (contact area growth plus formation of new chemical bonds between asperity contacts at the sub-microscale)[5,11–16] and, (3) a combination of the two[17]. The underlying mechanism of fault frictional healing is generally attributed to an increase in the real contact area of the microscopic asperities (contact "quantity")[18,19] or an increase in contact strength of chemical bonds (contact "quality")[15,20]. Although specific mechanisms differ, laboratory studies on centimeter-size rock specimens, mostly conducted at room temperature, and micro-scale single asperity friction tests have shown that 1) frictional healing (static friction minus dynamic steady-state friction, Fig. 1) usually increases linearly with the logarithm of the hold time t_h, and 2) the rate of healing (change of frictional healing with $\log(t_h)$) is positive for a broad range of rock types, including Westerly granite, and a variety of minerals[11,14–17,21–25]. However, the results of recent experiments also conducted on Westerly granite, but under hydrothermal conditions, cast doubt on

[1]Department of Geosciences, University of Padova, Padua, Italy. [2]State Key Laboratory of Earthquake Dynamics and Forecasting, Institute of Geology, China Earthquake Administration, Beijing, China. [3]Applied Mechanics Laboratory and Department of Engineering Mechanics, Tsinghua University, Beijing, China. [4]Istituto Nazionale di Geofisica e Vulcanologia, Rome, Italy. [5]Present address: GFZ Helmholtz Centre for Geosciences, Potsdam, Germany. [6]These authors contributed equally: Wei Feng, Wenzhou Wang, Lu Yao. ✉e-mail: luyao@ies.ac.cn; qunyang@tsinghua.edu.cn; giulio.ditoro@unipd.it

https://doi.org/10.1038/s41467-025-67521-x

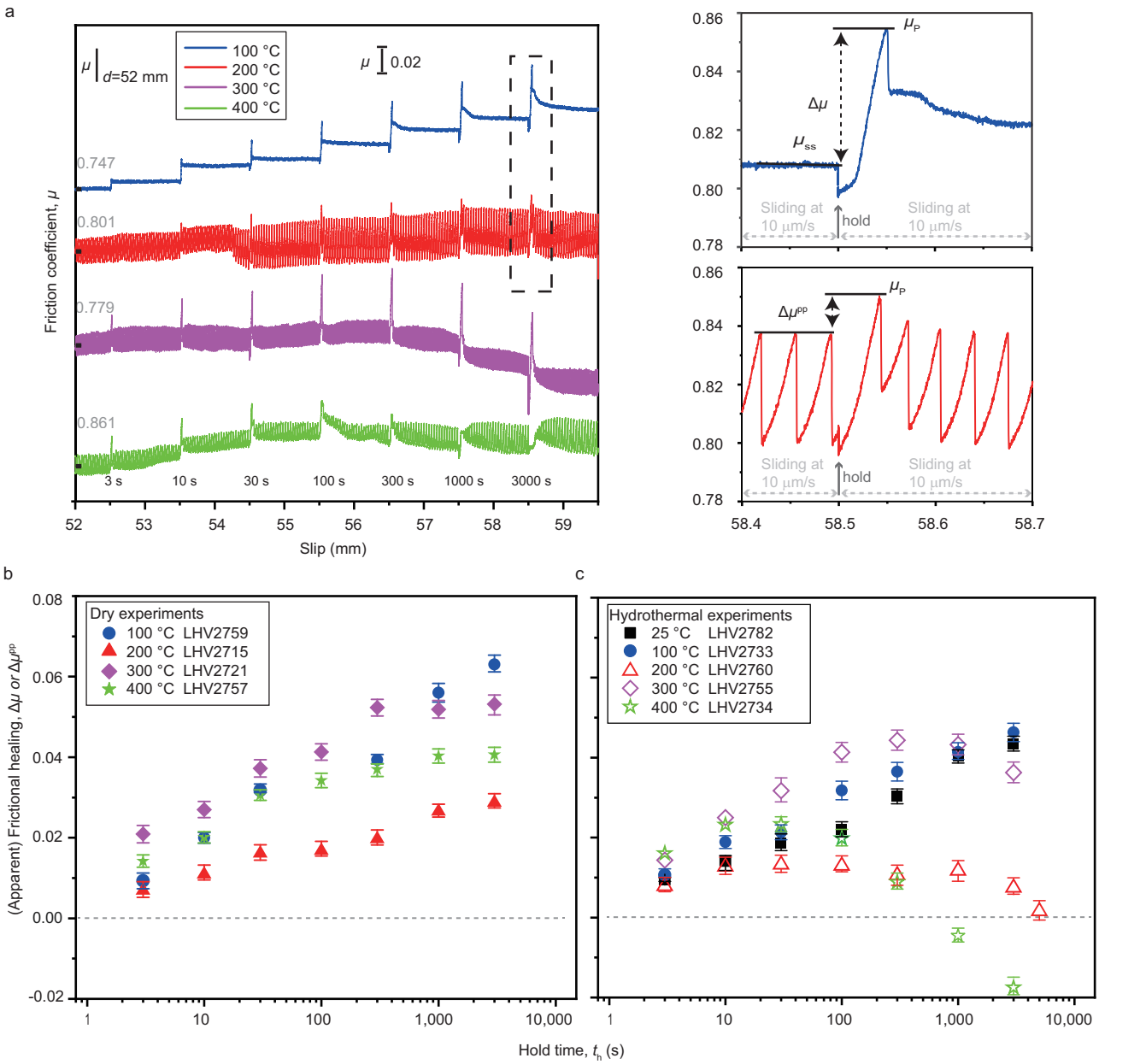

Fig. 1 | Experimental protocol for slide-hold-slide (SHS) tests and results of gabbro under hydrothermal conditions. a Friction coefficient μ versus displacement in the second SHS sequence (SHS-seq 2; slip rate = 10 μm/s) for four representative experiments (LHV2733, LHV2760, LHV2755 and LHV2734) performed at temperatures of 100 °C (top curve) to 400 °C (bottom curve) and pore fluid pressure of 30 MPa. Hold times (t_h) are indicated below each corresponding hold. Frictional healing $\Delta\mu$ and apparent healing $\Delta\mu^{pp}$ (see insets in the right panel of **a**) are determined by the difference between peak friction (μ_p) after the hold and steady-state friction (μ_{ss}) before the hold ($\Delta\mu = \mu_p - \mu_{ss}$) for stable slip and by the difference between peak friction before and after the hold for stick slip, respectively. The numbers on the left edge of the left panel of **a** indicate μ at a slip displacement of 52 mm. Insets in the right panel show the details of the 3000 s hold at T = 100 °C (top) and 200 °C (bottom). **b** Frictional healing data ($\Delta\mu$ or $\Delta\mu^{pp}$) of SHS-seq 2 under dry conditions. **c** Frictional healing data ($\Delta\mu$ or $\Delta\mu^{pp}$) of SHS-seq 2 under hydrothermal conditions, see main text for description. Solid symbols denote $\Delta\mu$ and open symbols denote $\Delta\mu^{pp}$. Error bar in b and c represent the standard deviation of the data (see Methods).

the occurrence of this log-linear frictional behavior: at T = 200 °C, frictional healing decreases, rather than increases, with log(t_h) (i.e., negative healing rate), although the healing is still positive within the investigated hold times. But, at T = 250 °C, the frictional healing becomes negative when hold time is longer than a threshold[26].

Consequently, faults in granitoids in the presence of hot and pressurized fluids, a common situation at hypocentral depths[4,27], may have negative healing rates, which will alter the seismic cycle. But do other common crustal rocks have similar frictional healing behavior under hydrothermal conditions? And what is the mechanism for the negative healing rate?

In this work, we measure the frictional healing behavior of a wide range of common crustal rocks at temperatures typical of hypocentral depths. We show that the negative healing rate behavior is closely related to the presence of feldspar and water. The key role played by feldspar in the process of decreasing fault frictional healing rate is confirmed by nanometer-scale friction experiments with a single feldspar micro-grain translating along a feldspar substrate using an

https://doi.org/10.1038/s41467-025-67521-x

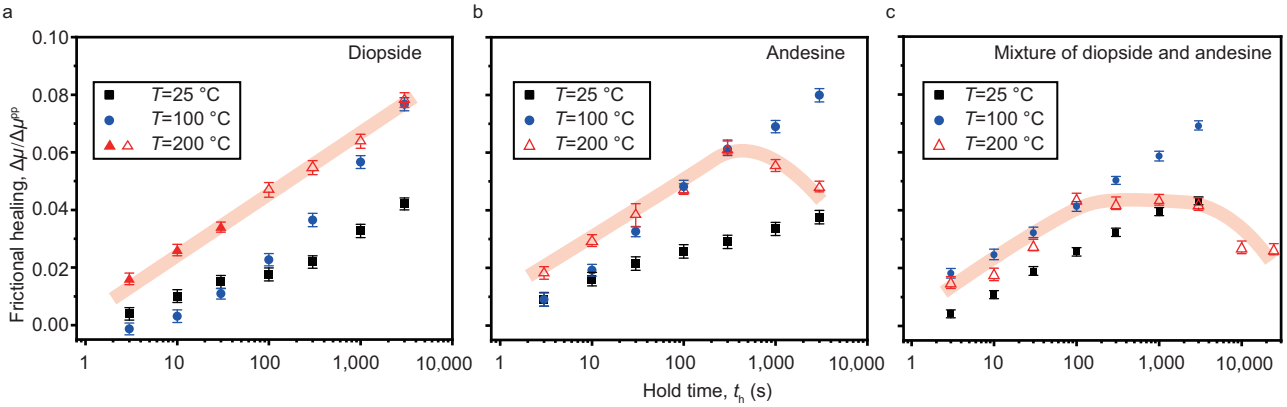

Fig. 2 | Frictional healing data for the primary rock-forming minerals of gabbro. Experiments are performed under an effective normal stress (σ_{eff}) of 50 MPa, temperature (T) ranging from 25 °C to 200 °C and pore fluid pressure (P_p) of 30 MPa. Error bar represents the standard deviation of (apparent) $\Delta\mu$. **a** Diopside data from experiment LHV3099. Frictional healing ($\Delta\mu$) increases linearly with logarithm of hold time ($\log_{10}t_h$) at all temperatures investigated (T = 25 to 200 °C). **b** Andesine data from experiment LHV3100. At T = 25 and 100 °C, $\Delta\mu$ increases monotonically with $\log_{10}(t_h)$, whereas at T = 200 °C, $\Delta\mu$ decreases with increasing hold time at t_h > 300 s. **c** Analog of gabbro gouge, i.e., mixture of diopside and andesine with a ratio of 1:1.68 from experiment LHV3103. Frictional healing behavior of the mixture is similar to that of pure andesine. These experiments suggest that the presence of andesine is responsible for the decreased frictional healing and negative healing rate observed for long-duration holds. The trend of $\Delta\mu$ with $\log_{10}t_h$ at T = 200 °C are highlighted in shaded lines. Solid symbols denote friction healing $\Delta\mu$ and open symbols denote apparent healing $\Delta\mu^{pp}$.

atomic force microscope. We conclude that thermally-activated and water-assisted chemical processes operating along feldspar interfaces limit the rate of contact strengthening, thereby reducing fault frictional healing.

Results

Frictional healing $\Delta\mu$ is normally investigated by laboratory slide-hold-slide (SHS) experiments[11,19,22]. Here we present results of 30 SHS experiments performed in the presence of hot and pressurized water using a rotary shear machine (LHV-Beijing) equipped with a dedicated hydrothermal pressure vessel[28–30] (Supplementary Fig. 1 and Supplementary Table 1).

We first report frictional healing data for powders of gabbro, a common oceanic crust rock. Experiments are performed under an effective normal stress ($\sigma_{eff} = \sigma_n - P_p$) of 50 MPa, a loading velocity of 10 µm/s, temperature (T) ranging from 25 to 400 °C and pore fluid pressure (P_p) of 0 (nominally dry, relative humidity < 2% at $T \geq 100$ °C) or 30 MPa. Each experiment includes two identical SHS sequences (SHS-seq 1 and SHS-seq 2) with a slip interval of 40 mm in between (see the representative experiment LHV2760 in Supplementary Fig. 2). The SHS procedure involves: (1) sliding at V = 10 µm/s for 1 mm of slip displacement, (2) holding at zero load-point velocity for hold times (t_h) ranging from 3 s to 10,000 s, and (3) resuming the sliding at the original velocity (V = 10 µm/s). Figure 1a shows the evolution of the friction coefficient ($\mu = \tau/\sigma_{eff}$, with τ the shear stress) with slip displacement (d ~ 52-59.5 mm) in the SHS-seq 2 for experiments performed at temperatures of 100 °C to 400 °C. At these loading and temperature conditions the rheology of gabbro and its forming minerals is elasto-frictional[31]. Typically, frictional healing $\Delta\mu$ is measured as the difference between peak μ value (μ_p) upon re-sliding and steady state friction (μ_{ss}) before the hold. However, in the cases of stick-slip, a well-defined μ_{ss} cannot be obtained. We adopt the peak friction during the stick phase before the hold as a reference point. The apparent $\Delta\mu$ is then measured as the difference between the peak μ value of the stick-slip events after and before the holds (see Methods; referred to as $\Delta\mu^{pp}$, Fig. 1a inset). The rate of healing (β) is conventionally determined as the slope of $\Delta\mu$ versus $\Delta\log_{10}(t_h)$ over the entire dataset, expressed as $\beta = \Delta\mu/\Delta\log_{10}t_h$[19]. Since some of the datasets in our study cannot be adequately described by a single log-linear relation, we determine individual healing rates (β^{loc}) within intervals of monotonic change to explicitly capture the time-dependent evolution of β. Typically, two β^{loc} values are sufficient to describe the change of $\Delta\mu$ with hold time. A positive β^{loc} indicates that frictional healing increases with hold time, whereas a negative β^{loc} indicates that frictional healing decreases with hold time.

Gabbro shows different healing behaviors in the presence or absence of pressurized water. Here we focus on the frictional healing behavior of SHS-seq 2 (results of SHS-seq 1 can be found in Supplementary Fig. 3). Under dry conditions, β is positive and $\Delta\mu$ generally increases monotonically with $\log_{10}t_h$ except for a slight deviation from the log-linear trend at T = 300 °C and 400 °C at longer hold times (≥ 1000 s) (Fig. 1b). For the experiments in the presence of water (P_p = 30 MPa), at T = 25 °C and 100 °C, $\Delta\mu$ increases linearly with $\log_{10}t_h$, as observed under dry conditions. However, at $T \geq 200$ °C, the linear relation between apparent $\Delta\mu$ and $\log_{10}t_h$ does not hold. Specifically, at 200 °C apparent $\Delta\mu$ starts to decrease with increasing t_h when t_h > 300 s, indicating that frictional healing rate has switched from positive ($\beta^{loc} > 0$) to negative ($\beta^{loc} < 0$) values. For the test at T = 400 °C, the negative transition of frictional healing rate ($\beta^{loc} < 0$) occurs at t_h = 100 s. Most strikingly, the peak μ value after the 3000 s hold is lower than the sliding μ before the hold, suggesting a negative value of apparent $\Delta\mu$ (Fig. 1c).

The transition in healing rates from positive to negative with increasing hold time apparently results from a reduction in (apparent) $\Delta\mu$ at longer hold times. In order to check whether or not the decrease in frictional healing at long hold times depends on the order in which the hold time is applied, we performed experiment LHV3047 at T = 200 °C by applying an increasing (3–3000 s) and decreasing (3000–3 s) order of hold time sequence. We find that both sequences produce a very similar pattern of healing behavior, as shown in Supplementary Fig. 4. This observation demonstrates that the decrease in $\Delta\mu$ at longer t_h is independent of hold sequence, and depends solely on the absolute duration of individual hold prior to the re-sliding.

X-ray diffraction (XRD) analysis of gabbro indicate that its mineralogical composition consists mainly of 47 wt% andesine and 28 wt% diopside (Supplementary Table 2, see Methods). To investigate whether the unusual frictional healing behavior of gabbro is sensitive to its mineral composition, we performed similar SHS experiments but on pure andesine and diopside gouges. These gouges are prepared by selecting the two minerals from gabbro gouges under the optical

microscope. We find that pure diopside gouges have a linear relationship between $\Delta\mu$ and $\log_{10}t_h$ under all investigated conditions (positive β, Fig. 2a). In contrast, pure andesine and a mixture of andesine and diopside with a ratio of 1.68:1 (or 47/28, same as in gabbro) show the same pattern of healing at 200 °C, including the occurrence of negative β after long t_h, as that of gabbro (Fig. 2b, c). These experiments indicate that the presence of andesine is responsible for the decreased $\Delta\mu$ and the negative β at long holds in the presence of pressurized water. To further demonstrate the role of temperature in the negative frictional healing rate, we conducted an additional SHS experiment LHV3240 on pure andesine gouge. The experiment includes three temperature sequences: two room temperature stages separated by a $T = 200$ °C stage. We observe the behavior of negative healing rate only in the $T = 200$ °C stage, not in the initial and final room temperature stages (Supplementary Fig. 5).

If andesine indeed accounts for the reduction in healing rate at elevated temperature conditions, we would expect this effect to occur in other types of feldspar and feldspar-rich rocks. To test this hypothesis, we present the fault frictional healing data for various feldspars, i.e., albite (Na-rich), orthoclase (K-rich) and andesine (Na-Ca rich) and feldspar-rich rocks (Etna basalt: 34% andesine + 11.3% sanidine, diorite: 49% albite, and Westerly granite: 35% albite + 19% microcline). As shown in Fig. 3, all types of feldspar and feldspar-rich rocks investigated exhibit the same time-dependent, negative frictional healing rate (i.e., frictional healing rate transiting from positive to negative) after long holds at temperature above 200 °C to 300 °C, in contrast to constant, positive healing rate at lower temperatures (Supplementary Fig. 6). Mechanical data from these common (non-altered) crustal rocks further support the critical role of feldspar in producing negative frictional healing rates at long holds.

Discussion

Mechanism for negative frictional healing rate

Our experiments reveal an unexpected frictional healing behavior, where the log-linear relation between frictional healing (apparent) $\Delta\mu$ and stationary contact time t_h does not hold within the investigated hold durations at hydrothermal conditions with temperatures above 200 °C–300 °C or ambient conditions typical for the nucleation of crustal earthquakes[4,27]. Importantly we show that the negative frictional healing rate β^{loc} occurs in several and very common feldspar-rich rocks and demonstrate that this behavior is related to the presence of feldspars and pressurized hot water (Figs. 1–3). Thus, the negative frictional healing rate could be common in the seismogenic upper crust and impact the seismic cycle. This frictional healing behavior is in sharp contrast to the well-known linear dependence of $\Delta\mu$ with $\log_{10}t_h$ (positive β) in most cases[5,11] and negligible $\Delta\mu$ for clay-rich samples[32]. In our experiments at $T = 200$ °C, β switches from positive to negative when t_h exceeds a threshold (~ 300 s). This suggests an unidentified mechanism involving water-assisted and time- and temperature-dependent microscale weakening processes along the contact interfaces of feldspar grains during the hold period.

A similar negative β value ($\beta^{loc} < 0$) has been reported recently for granite (46% feldspar) at $T \geq 200$ °C (reproduced experimental results can be found in Supplementary Fig. 7) and the mechanism was attributed to the formation of weak secondary minerals (clays)[26]. However, XRD and FESEM investigations conducted on gouge samples from experiments conducted at $T = 200$ °C that exhibit negative β do not show evidence of formation of new clays (Supplementary Fig. 8). This could be due to the low reaction rate of feldspar breakdown to form measurable (XRD) and visible (FESEM) amounts of clays at $T = 200$ °C within the duration of the experiments. But we cannot rule out the possibility that trace amounts of weak minerals may form locally in highly stressed contact asperities and are subsequently destroyed or displaced upon re-sliding. Previous experiments performed on gabbro[33] have reported that clay may form at $T = 300$ °C and 400 °C, and it is therefore likely that formed clay at original silicate mineral surface may contribute to the reduction in healing rate observed at $T \geq 300$ °C.

Time-dependent fault frictional healing has been attributed to an increase in real area of contacts with time (ΔA_r, contact "quantity") by asperity creep[18]. Friction experiments under atomic force microscope (AFM) suggest that an increase in contact strength of asperities ($\Delta\tau_a$, contact "quality") by the formation of stronger chemical bonds could be another potential mechanism for frictional healing[15]. The real area of contact in gouge sample can be described as a collection of discrete contact asperities and increases over time when two surfaces are in quasi-stationary contact[18,34,35]. Although direct observation of the real contact area in our experiments is unachievable, we measure the compaction of gouge layers during all holds and independently of temperatures and the presence of water (Supplementary Fig. 9), suggesting that the contact area increases even for samples with decreased frictional healing at long holds. Since the increase in ΔA_r cannot account for the decrease in $\Delta\mu$ during the long holds for feldspar-rich rocks, we must conclude that the growth rate of contact quality $\Delta\tau_a$ decreases during long holds[36].

Because the gouge friction experiment typically involves myriads of asperities of minerals (also with different composition) that come into contact, rotate and break during sliding, it is technically difficult to determine the shear strength of individual nano- to micro-contacts from the overall system responses. To better explore and illustrate the evolution of frictional strength during the healing experiments, we perform nano-scale contact[37] SHS experiments using an atomic force microscope (AFM). For the SHS experiments, an individual mineral grain, either feldspar or pyroxene, is mounted to the AFM cantilever and the lateral force is measured by sliding the individual mineral on a substrate of the same type of mineral at room temperature under relatively high humidity (RH ~ 80%, Fig. 4a). We vary the hold time from 3 s to 700 s and repeatedly measure frictional healing for 10 times under each hold time. As shown in Fig. 4 and Supplementary Fig. 10, the frictional healing behavior of the pyroxene-pyroxene contact pair and the feldspar-feldspar contact pair appears to be different. For the pyroxene-pyroxene contacts, the relative friction healing $\Delta F/F_{ss}$ (F_{ss}: steady state friction after hold; ΔF: peak friction after hold minus F_{ss}) increases log-linearly with t_h (Fig. 4b). In contrast, at the same RH ~ 80%, the variation of $\Delta F/F_{ss}$ with log (t_h) for feldspar-feldspar contacts has a much more pronounced scattering, particularly for $t_h > 30$ s. To better quantify the healing behaviors of the feldspar-feldspar contacts, we categorize the frictional healing data into two regimes, i.e., the "expected" healing and the "suppressed" healing. To do that, we first estimate the scattering of the frictional healing data of the pyroxene–pyroxene contacts as a reference scattering, as indicated by the width of the blue-shaded area in Fig. 4b. Then we find the trendline of the "expected" healing behavior for the feldspar-feldspar contacts by fitting the maximum frictional healing values under different hold times using a log-linear fit. Finally, we obtain the expected healing regime (denoted by the blue-shaded area) by considering the "expected" trendline with a same scattering as the pyroxene–pyroxene contacts. Essentially, this "expected" healing regime for the feldspar-feldspar contacts is defined as the projection of the normal log-linear healing behavior while considering a scattering due to uncertainty of the measurement system. Clearly, for the frictional healing measured in RH ~ 80%, many of the data points do not fall into the "expected" healing regime. For those data points that lie below the "expected" healing regime, we classify as the "suppressed" healing regime (denoted by the pink-shaded area, Fig. 4b). Taking the data set of 100 s hold time as an example (10 points in total), only one of the data points lie in the expected healing regime while the nine data points are in the suppressed healing regime. Similar behavior is more evident for the data sets of 300 and 700 s long holds, where 9 out of 10 data points and 10 out of 10 data points are in the suppressed healing regime,

https://doi.org/10.1038/s41467-025-67521-x

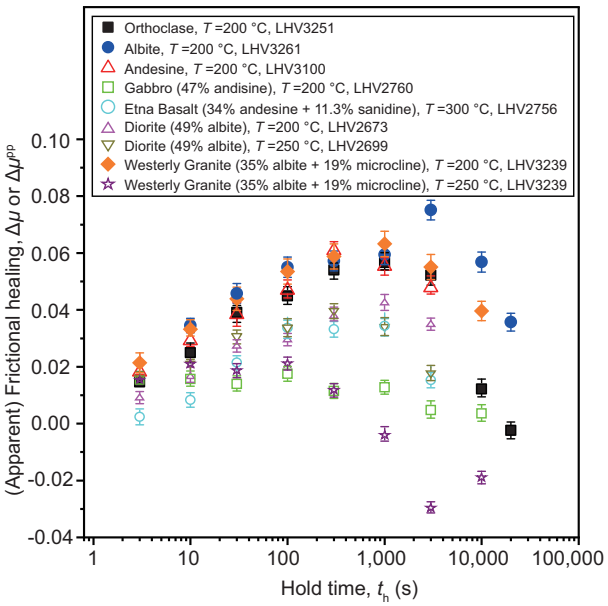

Fig. 3 | Frictional healing data for feldspars and common crustal feldspar-rich rocks. Experiments are performed at constant effective normal stress of 50 MPa and pore fluid pressure of 30 MPa. This plot shows that all investigated types of feldspars and feldspar-rich rock powders exhibit a similar pattern in frictional healing versus hold time at elevated temperatures ($T \geq 200$ °C). A positive healing rate switches to negative with increasing hold time. Error bar represents the standard deviation of $\Delta\mu$. Solid symbols denote friction healing $\Delta\mu$ and open symbols denote apparent healing $\Delta\mu^{pp}$.

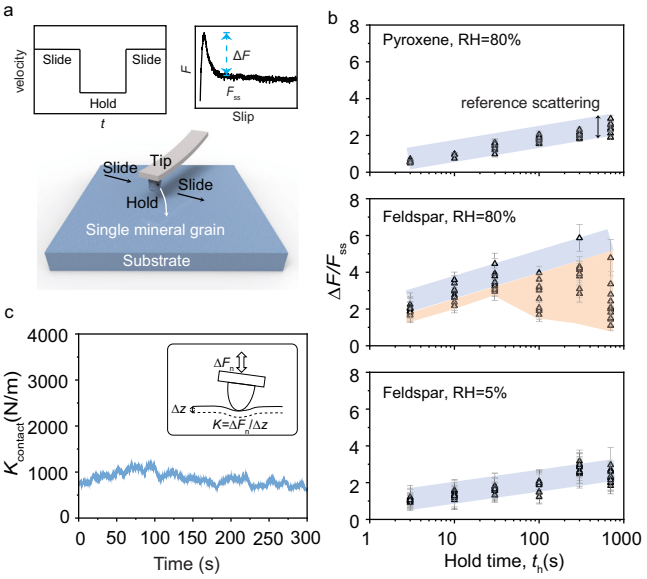

Fig. 4 | Single-component particle slide-hold-slide tests performed in Atomic Force Microscope (AFM). a A schematic diagram showing that a feldspar/pyroxene particle attached to a tip slides against feldspar/pyroxene surface. SHS tests are conducted with the same protocol as rotary shear SHS experiments (left inset). Upon resliding after the hold, the lateral force increases abruptly to a peak value and then evolves to a steady-state value (F_{ss}). ΔF is determined by the difference between peak value and steady state value (right inset). **b** Normalized frictional healing data for the pyroxene-pyroxene contact at RH ~ 80% (upper panel), feldspar-feldspar contact at RH ~ 80% (middle panel) and at RH ~ 5% (lower panel). The blue shaded domain outlines the expected linear trend for $\Delta F/F_{ss}$ versus hold time. The pink shaded domain marks the "suppressed" frictional healing effect. Error bar presents the standard deviation of $\Delta F/F_{ss}$ (see Methods). **c** Evolution of the contact stiffness of the system (K) during a 300 s hold for the feldspar-feldspar contact. Inset shows a schematic diagram of the stiffness measurement. The K is the ratio of the normal force variation ΔF_n to the vertical displacement change Δz.

respectively. Most strikingly, in the 700 s long hold, some of the frictional healing values are even smaller than those collected in the 3 s long holds. We also perform SHS experiments for feldspar-feldspar contacts under relatively low humidity conditions (RH ~ 5%) and find that conventional frictional healing is more apparent than in high humidity SHS tests (Fig. 4b). The suppressed frictional healing for the feldspar-feldspar contacts after long hold times at high relative humidity (but not for the pyroxene-pyroxene contacts or the feldspar-feldspar contacts at low humidity) is consistent with our results for macro-scale gouge experiments in the presence of pressurized water[38] (Figs. 1–3).

Due to the instrumentational limitations of the AFM, it was not possible to conduct nano-scale SHS experiment at 200 °C or with pressurized water. However, we are still able to observe the suppressed frictional healing at room temperature in the feldspar-feldspar contacts, e.g. in 9 out of 10 data points for $t_h = 300$ s (Fig. 4b). Such observations are not surprising. As evident in the previous AFM experiments[15,37], the frictional healing effect and other interfacial phenomena are commonly more pronounced than those observed at the macroscale. For instance, individual contact healing (i.e., $\Delta F/F_{ss}$ up to ~6, Fig. 4b) is more pronounced than the equivalent quantity, $\Delta\mu/\mu_{ss}$, of ~ 0.1 for multiple-contact macroscale rotary shear experiments (Fig. 1). This high sensitivity is possibly due to the high local stress and good chemical uniformity for the nanoscale asperity contact. Nevertheless, probably because the ambient temperature in our AFM experiments was significantly lower than that in the rotary shear experiments, the suppressed frictional healing could not always occur at the nanoscale, despite the high interfacial sensitivity.

Since SHS experiments with AFM employ a single feldspar micrograin, this experimental approach offers a unique and simpler platform to examine the evolution of the contact interface during the hold period. We repeat the SHS experiments of the feldspar-feldspar contact for a long hold time ($t_h = 300$ s) under RH ~ 80% while in-situ monitoring the contact stiffness K of the system (Fig. 4c). The K is the ratio of the normal force variation ΔF_n to the vertical displacement change Δz[39]. During the 300 s long hold, there is no significant change in K, which means that the contact area does not change appreciably. Therefore, the suppressed friction healing effect during the longer hold times must be caused by a reduced growth rate in contact quality, relative to short holds, of the micro-grain contacts. Considering the statistical nature of the suppressed frictional healing effect and its close relation with humidity (a water bridge between the AFM tip and the substrate was likely to form under relatively high humidity[40,41]), we speculate that the process may be thermally activated, water-assisted and chemical in origin.

Implications for the seismic cycle

Our study reveals that feldspar and feldspar-rich rocks exhibit time-dependent reduction of frictional healing at temperatures ≥ 200°C, typical of depths greater than ~ 8 km assuming a geothermal gradient of 25 °C/km. These depths align well with hypocentral depths where earthquakes nucleate[4,42]. Therefore, this healing behavior may potentially influence the seismic cycle in feldspar-bearing faults. Our results suggest that extrapolating laboratory-derived healing parameters to predict the recurrence interval of earthquakes in feldspar-rich fault zones under hydrothermal conditions should be treated with caution, unlike the direct applications made in previous studies[11]. For instance, the decrease in frictional healing and healing rate will, if the stress loading rate remains constant, 1) reduce the rate of the elastic strain energy stored by wall rocks and, 2) the recurrence interval of earthquakes along this fault may become shorter, and subsequent

earthquakes may occur at a lower shear stress level[43]. The distribution of feldspar-rich patches along faults may influence the frequency of earthquakes and their stress drops.

Although the experiments discussed here highlight the role of the presence of feldspar in activating the negative frictional healing rate behavior in common crustal rocks, the extrapolation of laboratory frictional healing results to natural faults remains challenging. By comparison with conditions of natural fault systems, (1) the experiments presented here are of short duration and reaction kinetics are too slow to observe chemically-controlled contact weakening for minerals other than feldspar, (2) frictional healing properties of faults vary significantly with ambient temperature[13,23,26], fluid composition[44,45], and lithology[46,32], and (3) other relevant co- to post-seismic processes (e.g., vein precipitation, fault welding) contribute to fault healing[8,14]. In any case, our findings highlight the need to revisit fault frictional healing mechanisms under hydrothermal conditions, a very common situation at hypocentral depths. In particular, the presence of feldspar may lead to a decrease in fault strength recovery under ambient conditions discussed in this study. The changes in strength of the interfacial contacts during quasi-stationary state control frictional healing in feldspars. Our study suggests that the mechanism of frictional healing is governed by a combination of real area of contact and interfacial contact strength[15,18].

Methods

Hydrothermal friction experiments and slide-hold-slide tests

The sample powders used in the experiments include "Jinan dark green" gabbro, Westerly granite, Etna basalt, diorite, and orthoclase and albite. The mineralogical make up are presented in Supplementary Table 2, based on XRD data. The samples are crushed and sieved using a 180-mesh sieve to produce gouges with grain size <88 μm for the friction experiments.

Friction experiments are performed with a Low to High Velocity Rotary shear apparatus (LHVR-Beijing) equipped with a hydrothermal pressure vessel at the Institute of Geology, China Earthquake Administration in Beijing, China (Supplementary Fig. 1)[28–30]. All experiments are conducted at a constant effective normal stress (σ_{eff}) of 50 MPa and temperature (T) ranging from 25 to 400 °C, under nominally "dry" or with a pore fluid pressure (P_p) of 30 MPa. In the dry experiments, the vessel is open to the atmosphere. The P_p = 30 MPa experiments are conducted under drained conditions (distilled water as pore fluid) and constant pore pressure is maintained by a syringe ISCO pump. A list of all the experiments can be found in Supplementary Table 1.

In each experiment, a 1.5 mm thick gouge layer is sandwiched between two ring-shaped and surface-grooved holders and flanked by inner and outer metal rings (for 22/28 mm and 14/20 mm internal/external diameter, ~0.8 g and 0.56 g gouges are used, respectively). The sample assembly is subsequently mounted inside the hydrothermal vessel and to the machine. Then, the sample assembly and the vessel are evacuated to 2000 Pa with a vacuum pump. Afterward, the normal stress σ_n is slowly increased to the desired value, while the pore fluid pressure (P_p) is increased in a stepped manner and kept at a constant target value before heating. Once the desired pore pressure and normal stress are achieved, the vessel is heated to target temperature. Heating normally takes 30 min for T = 100 °C and ~1.5 h for T = 400 °C.

After achieving the desired experimental conditions, the gouge layer is sheared (run-in) at V = 10 μm/s for 7 mm slip displacement (d), allowing friction to evolve to a steady state value. After this "run-in" stage, slide-hold-slide tests are imposed. The SHS test consists of three steps: (1) sliding the gouge layer at V = 10 μm/s for 1 mm of slip displacement, (2) holding the gouge for hold times (t_h) ranging from 3 s to 30,000 s by setting the load point velocity as null and, (3) resuming the sliding velocity at the original rate (V = 10 μm/s). Upon reloading, the friction coefficient typically reaches a peak value and then decays to a steady state value. Frictional healing $\Delta\mu$ is defined as the difference between μ peak value (μ_p) upon re-sliding and steady state friction (μ_{ss}) before the hold. For stable sliding, μ_{ss} is calculated as the average values of μ (with standard error) measured over the last 0.2 mm of displacement before the hold. In the cases of stick-slip, a μ_{ss} counterpart is determined by averaging peak μ values (with standard error) during the stick phases within the last 0.2 mm of displacement (normally 6–8 cycles). It is worth noting that the measurement of $\Delta\mu$ in the case of stick slip is not affected by where the hold happens to start in the loading curve (Supplementary Fig. 11). Normal stress is kept constant during the holds and frictional strength relaxes non-linearly due to the creep of the machine and gouge samples. To ensure that no rotation is applied by the machine to the gouge layer during holds, the servo motor control system is set to stop once the imposed revolution rate is less than 1 rpm (corresponding to a slip velocity ~ 1.3 μm/s for the sample assembly used). By doing so, the servo motor remains stopped even if zero-voltage input signal is disturbed by electric noise, and no angular rotation is detected during the holds. In each experiment, two SHS sequences separated by a slip displacement of 40 mm are imposed. At the end of the experiment, the deformed samples are collected for micro-analytical (XRPD and FESEM) investigations. Note that the samples required a cooling period of approximately 1 h for T = 200 °C before being removed, this process might have potentially modified the microstructures.

During the experiments, axial load, shear torque, fluid pressure and temperature, velocity, revolution, and axial displacement are acquired at a frequency of 100 Hz. Evolution of axial displacement, i.e., dilatation or shortening (Δw) of the gouge layer, is recorded using a LVDT (1 μm resolution and 10 mm stroke) placed on the axial column of the machine. No correction for system stiffness is applied for the calculation of the shear displacement. The measured shear torque is converted to shear stress (MPa) without correcting for the additional shear resistance from O-rings and confining rings.

Atomic force microscopy and slide-hold slide tests

Sample preparation. Feldspar/Pyroxene tips are fabricated from tipless atomic force microscopy (AFM) probes and mineral particles. The feldspar/pyroxene particles, separated from the samples used in rotary shear experiments, are attached to tipless AFM probes (HQ-NSC35 Mikromasch) using UV (ultraviolet) glue. The selected feldspar and pyroxene particles have a diameter of several tens of micrometers. The solid gabbro substrate is polished by Argon Ion Polishing, producing a smooth surface with a root-mean-square roughness of 3.0 nm, measured within an area of 4 × 4 μm^2. The gabbro substrate is cleaned with air plasma beam before each experiment.

AFM experiments. Friction force microscopy is conducted using an AFM (Ntegra, NT-MDT Inc.) installed at the Tsinghua University, China. The experiments are conducted in an AFM chamber at approximately 80% humidity. The humidity is kept constant (uncertainty ±2% RH) controlled by bubbling pure dry nitrogen vapor from a liquid nitrogen dewar through water. The experimental system is equilibrated for at least 1 h after the initial humidity change.

The friction experiments are performed after initially making contact between the feldspar/pyroxene tip and the substrate, then sliding for a run-in distance (256 cycles of 1 μm back-and-forth lateral displacements). The slide-hold-slide procedure is then conducted at a constant normal load of 150 nN. The tip is first slid 1 μm, then held stationary for a set time, followed by sliding another 1 μm at the original velocity. After this, the tip is slid backward to the original position. The friction was determined by calculating the difference between the forward and backward lateral forces. The hold time is predetermined ranging from 3 s to 700 s. Each hold time sequence is repeated 10 times. To exclude the potential effect caused by different interfacial chemical states, the tip is slid for a pre-run distance before each different hold time.

The healing of friction is described as normalized friction force increment, called the relative friction drop $\Delta F/F_{ss}$, which is the ratio of the increment of friction force during the hold stage (ΔF) and the steady-state friction (F_{ss}) after the hold. To estimate the uncertainty of $\Delta F/F_{ss}$ for each hold event, we first determined the peak force value (F_p) and subtracted from it the individual force values (F_i) during post-hold steady-state sliding, thereby obtaining a dataset of $\Delta F_i = F_p - F_i$. Based on the ΔF_i and F_i datasets, we then calculated the mean value ($\bar{\Delta F}$ and $\bar{F_{ss}}$) and standard deviation ($\sigma_{\Delta F}$ and $\sigma_{F_{ss}}$) of ΔF and F_{ss}, respectively. Finally, the standard deviation of $\Delta F/F_{ss}$ was estimated using the error propagation formula:

$$\sigma_R = \frac{\bar{\Delta F}}{\bar{F_{ss}}}\sqrt{\left(\frac{\sigma_{\Delta F}}{\Delta F}\right)^2 + \left(\frac{\sigma_{F_{ss}}}{\bar{F_{ss}}}\right)^2} \quad (1)$$

X-ray powder diffraction (XRPD)

Measurements are performed using a Philips X'Pert Pro MPD diffractometer installed at the Department of Geosciences at the University of Padova, Italy. The instrument is equipped with a long-fine-focus cobalt anode tube working at 40 kV – 40 mA and a 240 mm goniometer radius that operates in the θ/θ geometry. Samples are prepared using the front-loading procedure onto a Si-crystal sample holder that lacks any diffraction lines (zero-background). Measurements for phase identification are carried out between 3° and 85° 2θ angle, using a 0.017° step size, counting 100 s per virtual step on a spinning sample (1 revolution per second).

Field Emission Scanning Electron Microscope (FESEM)

Measurements are conducted using a Tescan 468 Solaris Field-Emission SEM of the Department of Geosciences at the University of Padova. Backscattered electron images have been acquired with an in-beam mid-angle backscattered detector using an accelerating voltage of 5 KeV, current of 300 pA and a working distance of 3 or 4 mm.

Data availability

The mechanical data generated in this study has been deposited in Zenodo at https://zenodo.org/records/16754750. Source data are provided in the supplementary information. Source data are provided with this paper.

References

1. Brace, W. F. & Byerlee, J. D. Stick-slip as a mechanism for earthquakes. *Science* **153**, 990–992 (1966).
2. Reid, H. F. The California Earthquake of April 18, 1906: volume II (The Mechanics of the 281 Earthquake). *State Earthq. Investig. Com*. **192**, 165–166 (1910).
3. Brenguier, F., Campillo, M., Hadziioannou, C., Shapiro, N. M. & Larose, E. Postseismic relaxation along the San Andreas Fault at Parkfield from continuous seismological observations. *Science* **321**, 1478–1481 (2008).
4. Scholz, C. H. The Mechanics of Earthquakes and Faulting. (Cambridge University Press, 2019).
5. Dieterich, J. H. Time-dependent friction in rocks. *J. Geophys. Res.* **77**, 3690–3697 (1972).
6. Beeler, N. N., Tullis, T. E. & Weeks, J. D. The role of time and displacement in the evolution effect in rock friction. *Geophys. Res. Lett.* **21**, 1987–1990 (1994).
7. Di Toro, G. & Pennacchioni, G. Fault plane processes and mesoscopic structure of a strong-type seismogenic fault in tonalites (Adamello batholith, Southern Alps). *Tectonophysics* **402**, 55–80 (2005).
8. Mitchell, T. M., Toy, V., Di Toro, G., Renner, J. & Sibson, R. H. Fault welding by pseudotachylyte formation. *Geology* **44**, 1059–1062 (2016).
9. Brantut, N. & Viesca, R. C. Earthquake nucleation in intact or healed rocks. *J. Geophys. Res. Solid Earth* **120**, 191–209 (2015).
10. Masoch, S., Fondriest, M., Preto, N., Secco, M. & Di Toro, G. Seismic cycle recorded in cockade-bearing faults (Col de Teghime, Alpine Corsica). *J. Struct. Geol.* **129**, 103889 (2019).
11. Marone, C. The effect of loading rate on static friction and the rate of fault healing during the earthquake cycle. *Nature* **391**, 69–72 (1998).
12. Marone, C., Vidale, J. E. & Ellsworth, W. L. Fault healing inferred from time-dependent variations in source properties of repeating earthquakes. *Geophys. Res. Lett.* **22**, 3095–3098 (1995).
13. Barbot, S. A rate-, state-, and temperature-dependent friction law with competing healing mechanisms. *J. Geophys. Res. Solid Earth* **127**, e2022JB025106 (2022).
14. Bedford, J. D., Hirose, T. & Hamada, Y. Rapid fault healing after seismic slip. *J. Geophys. Res. Solid Earth* **128**, e2023JB026706 (2023).
15. Li, Q., Tullis, T. E., Goldsby, D. & Carpick, R. W. Frictional ageing from interfacial bonding and the origins of rate and state friction. *Nature* **480**, 233–236 (2011).
16. Thom, C. A., Carpick, R. W. & Goldsby, D. L. Constraints on the physical mechanism of frictional aging from Nanoindentation. *Geophys. Res. Lett.* **45**, 13306–13311 (2018).
17. Nakatani, M. & Scholz, C. H. Frictional healing of quartz gouge under hydrothermal conditions: 1. Experimental evidence for solution transfer healing mechanism. *J. Geophys. Res. B Solid Earth* **109**, 1–19 (2004).
18. Dieterich, J. H. & Kilgore, B. D. Direct observation of frictional contacts: New insights for state-dependent properties. *Pure Appl. Geophys* **143**, 283–302 (1994).
19. Marone, C. Laboratory-derived Friction Laws and their application to seismic faulting. *Annu. Rev. Earth Planet. Sci.* **26**, 643–696 (1998).
20. Liu, Y. & Szlufarska, I. Chemical origins of frictional aging. *Phys. Rev. Lett.* **109**, 186102 (2012).
21. Yasuhara, H., Marone, C. & Elsworth, D. Fault zone restrengthening and frictional healing: the role of pressure solution. *J. Geophys. Res.* **110**, B06310 (2005).
22. Carpenter, B. M., Ikari, M. J. & Marone, C. Laboratory observations of time-dependent frictional strengthening and stress relaxation in natural and synthetic fault gouges. *J. Geophys. Res. Solid Earth* **121**, 1183–1201 (2016).
23. Chen, J., Verberne, B. A. & Spiers, C. J. Interseismic re-strengthening and stabilization of carbonate faults by 'non-Dieterich' healing under hydrothermal conditions. *Earth Planet. Sci. Lett.* **423**, 1–12 (2015).
24. Karner, S. L., Marone, C. & Evans, B. Laboratory study of fault healing and lithification in simulated fault gouge under hydrothermal conditions. *Tectonophysics* **277**, 41–55 (1997).
25. Frye, K. M. & Marone, C. Effect of humidity on granular friction at room temperature. *J. Geophys. Res. Solid Earth* **107**, ETG 11-1–ETG 11-13 (2002).
26. Jeppson, T. N., Lockner, D. A., Beeler, N. M. & Moore, D. E. Time-dependent weakening of granite at hydrothermal conditions. *Geophys. Res. Lett.* **50**, 1–9 (2023).
27. Gomila, R. et al. Frictional melting in hydrothermal fluid-rich faults: field and experimental evidence from the Bolfín Fault Zone (Chile). *Geochemistry, Geophys. Geosystems* **22**, e2021GC009743 (2021).
28. Ma, S., Shimamoto, T., Yao, L., Togo, T. & Kitajima, H. A rotary-shear low to high-velocity friction apparatus in Beijing to study rock friction at plate to seismic slip rates. *Earthq. Sci* **27**, 469–497 (2014).
29. Feng, W. et al. Physical state of water controls friction of gabbro-built faults. *Nat. Commun.* **14**, 4612 (2023).
30. Yao, L. et al. Seismic fault slip at depths simulated by high-velocity friction experiments under hydrothermal conditions. *Proc. Natl. Acad. Sci.* **122**, e241570122 (2025).
31. He, C., Wang, Z. & Yao, W. Frictional sliding of gabbro gouge under hydrothermal conditions. *Tectonophysics* **445**, 353–362 (2007).

32. Carpenter, B., Marone, C. & Saffer, D. Weakness of the San Andreas fault revealed by samples from the active fault zone. *Nature Geosci.* **4**, 251–254 (2011).
33. Feng, W. et al. Slip-dependence of fault frictional stability under hydrothermal conditions. *Geophys. Res. Lett.* **51**, e2024GL108525 (2024).
34. Im, K., Elsworth, D. & Fang, Y. The influence of preslip sealing on the permeability evolution of fractures and faults. *Geophys. Res. Lett.* **45**, 166–175 (2018).
35. Im, K., Elsworth, D. & Wang, C. Cyclic permeability evolution during repose then reactivation of fractures and faults. *J. Geophys. Res. Solid Earth* **124**, 4492–4506 (2019).
36. Weber, B., Suhina, T., Brouwer, A. M. & Bonn, D. Frictional weakening of slip interfaces. *Sci. Adv.* **5**, eaav7603 (2019).
37. Li, S., Zhang, S., Chen, Z., Feng, X. & Li, Q. Length scale effect in frictional aging of silica contacts. *Phys. Rev. Lett.* **125**, 215502 (2020).
38. Dieterich, J. H. & Conrad, G. Effect of humidity on time- and velocity-dependent friction in rocks. *J. Geophys. Res.* **89**, 4196–4202 (1984).
39. Jarvis, S. P., Oral, A., Weihs,T. P. & Pethica, J. B. *Rev. Sci. Instrum*. **64**, 3515–3520 (1993).
40. Szoszkiewicz, R. & Riedo, E. Nucleation time of nanoscale water bridges. *Phys. Rev. Lett.* **95**, 135502 (2005).
41. Bocquet, L., Charlaix, E., Ciliberto, S. & Crassous, J. Moisture-induced ageing in granular media and the kinetics of capillary condensation. *Nature* **396**, 735–737 (1998).
42. Bonner, J. L., Blackwell, D. D. & Herrin, E. T. Thermal constrains on earthquake depths in California. *B. Seismol. Soc. Am.* **93**, 2333–2354 (2003).
43. Wimpenny, S., Forrest, N. & Copley, A. Time dependence decrease in fault strength in the 2011-2016 Ibarak-Fukushima earthquake sequence. *Geophys. J. Int.* **232**, 788–809 (2023).
44. Mizoguchi, K., Takahashi, M., Masuda, K. & Fukuyama, E. Fault strength drop due to phase transitions in the pore fluid. *Geophy. Res. Lett.* **34**, L09313 (2007).
45. Moore, D. E. & Lockner, D. A. Chemical controls on fault behavior: Weakening of serpentinite sheared against quartz-bearing rocks and its significance for fault creep in the San Andreas system. *J. Geohys. Res. Solid Earth* **118**, 2558–2570 (2013).
46. Niemeijer, A. R. & Spiers, C. J. Velocity dependence of strength and healing behaviour in simulated phyllosilicate fault gouge. *Tectonophysics* **427**, 231–253 (2006).

Acknowledgements

This study was financially supported by the National Natural Science Foundation of China (grants 42422408 and 42174223 to L.Y., grant 12025203 to Q.L. and grant U1839211 to S.M.), the State Key Laboratory of Earthquake Dynamics and Forecasting (Open Research Fund LED2024b09 to W.F.) and the Italian Ministry of University and Research (grant PRIN 2022WE2JY9 SCHOTTA to G.D.T., R.G. and W.F.). Elena Spagnuolo, Chaoqun Yang and Changrong He are thanked for providing samples. Marco Favero and Xi Ma are thanked for technical support. Chris Spiers, Yuntao Ji, Baoning Wu, Nicolas Brantut, Raphael Affinito, Lining Cheng, Telemaco Tesei, Kai Qu, Peng Yuan, Yanjuan Wang, Qingao Wang and Ting Li are thanked for discussions.

Author contributions

W.F., L.Y., Q.L., and G.D.T. conceived the study. W.F. and L.Y. performed the rock experiments. W.W. and Q.L. performed the AFM experiments. W.F. and L.Y. carried out the microstructural analysis with inputs from R.G. and G.D.T. W.F. wrote the first draft of the manuscript with inputs from W.W., L.Y., S.M., Q.L., and G.D.T. All authors discussed and interpreted the results.

Competing interests

The authors declare no competing interests.

Additional information

Supplementary information The online version contains supplementary material available at https://doi.org/10.1038/s41467-025-67521-x.

Correspondence and requests for materials should be addressed to Lu Yao, Qunyang Li or Giulio Di Toro.

Peer review information *Nature Communications* thanks Tamara Jeppson, Andreas Kronenberg and the other, anonymous, reviewer(s) for their contribution to the peer review of this work. A peer review file is available.